Nuclear Inst. and Methods in Physics Research B 457 (2019) 44–48

Contents lists available at ScienceDirect

Nuclear Inst. and Methods in Physics Research B

journal homepage: www.elsevier.com/locate/nimb

A ~100 μm-resolution position-sensitive detector for slow positronium

C. Amsler[c], M. Antonello[b,d], A. Belov[t], G. Bonomi[f,g], R.S. Brusa[h,i], M. Caccia[b,d], A. Camper[j], R. Caravita[j,*], F. Castelli[b,k], G. Cerchiari[l], D. Comparat[m], G. Consolati[n,b], A. Demetrio[o], L. Di Noto[p,q], M. Doser[j], M. Fanì[j,p,q], R. Ferragut[a,b], J. Fesel[j], S. Gerber[j], M. Giammarchi[b], A. Gligorova[c], F. Guatieri[h,i], P. Hackstock[c], S. Haider[j], A. Hinterberger[j], A. Kellerbauer[l], O. Khalidova[j], D. Krasnický[q], V. Lagomarsino[p,q], P. Lebrun[s], C. Malbrunot[j,c], S. Mariazzi[i,h,*], V. Matveev[t,e], S.R. Müller[o], G. Nebbia[u], P. Nedelec[s], M. Oberthaler[o], E. Oswald[j], D. Pagano[f,g], L. Penasa[h,i], V. Petracek[v], F. Prelz[b], M. Prevedelli[w], B. Rienaecker[j], J. Robert[m], O.M. Røhne[r], A. Rotondi[g,x], H. Sandaker[r], R. Santoro[b,d], G. Testera[q], I.C. Tietje[j], E. Widmann[c], T. Wolz[j], P. Yzombard[l], C. Zimmer[j,l,y], N. Zurlo[g,z]

[a] LNESS, Department of Physics, Politecnico di Milano, via Anzani 42, 22100 Como, Italy
[b] INFN Milano, via Celoria 16, 20133 Milano, Italy
[c] Stefan Meyer Institute for Subatomic Physics, Austrian Academy of Sciences, Boltzmanngasse 3, 1090 Vienna, Austria
[d] Department of Science, University of Insubria, Via Valleggio 11, 22100 Como, Italy
[e] Joint Institute for Nuclear Research, Dubna 141980, Russia
[f] Department of Mechanical and Industrial Engineering, University of Brescia, via Branze 38, 25123 Brescia, Italy
[g] INFN Pavia, via Bassi 6, 27100 Pavia, Italy
[h] Department of Physics, University of Trento, via Sommarive 14, 38123 Povo, Trento, Italy
[i] TIFPA/INFN Trento, via Sommarive 14, 38123 Povo, Trento, Italy
[j] Physics Department, CERN, 1211 Geneva 23, Switzerland
[k] Department of Physics "Aldo Pontremoli", University of Milano, via Celoria 16, 20133 Milano, Italy
[l] Max Planck Institute for Nuclear Physics, Saupfercheckweg 1, 69117 Heidelberg, Germany
[m] Laboratoire Aimé Cotton, Université Paris-Sud, ENS Paris Saclay, CNRS, Université Paris-Saclay, 91405 Orsay Cedex, France
[n] Department of Aerospace Science and Technology, Politecnico di Milano, via La Masa 34, 20156 Milano, Italy
[o] Kirchhoff Institute for Physics, Heidelberg University, Im Neuenheimer Feld 227, 69120 Heidelberg, Germany
[p] Department of Physics, University of Genova, via Dodecaneso 33, 16146 Genova, Italy
[q] INFN Genova, via Dodecaneso 33, 16146 Genova, Italy
[r] Department of Physics, University of Oslo, Sem Sælandsvei 24, 0371 Oslo, Norway
[s] Institute of Nuclear Physics, CNRS/IN2p3, University of Lyon 1, 69622 Villeurbanne, France
[t] Institute for Nuclear Research of the Russian Academy of Science, Moscow 117312, Russia
[u] INFN Padova, via Marzolo 8, 35131 Padova, Italy
[v] Czech Technical University, Prague, Brehová 7, 11519 Prague 1, Czech Republic
[w] University of Bologna, Viale Berti Pichat 6/2, 40126 Bologna, Italy
[x] Department of Physics, University of Pavia, via Bassi 6, 27100 Pavia, Italy
[y] Department of Physics, Heidelberg University, Im Neuenheimer Feld 226, 69120 Heidelberg, Germany
[z] Department of Civil, Environmental, Architectural Engineering and Mathematics, University of Brescia, via Branze 43, 25123 Brescia, Italy

ARTICLE INFO

Keywords:
Positronium
Imaging

ABSTRACT

In this work we describe a high-resolution position-sensitive detector for positronium. The detection scheme is based on the photoionization of positronium in a magnetic field and the imaging of the freed positrons with a Microchannel Plate assembly. A spatial resolution of (88 ± 5) μm on the position of the ionized positronium –in the plane perpendicular to a 1.0 T magnetic field– is obtained. The possibility to apply the detection scheme for monitoring the emission into vacuum of positronium from positron/positronium converters, imaging posi-

* Corresponding authors.
E-mail addresses: ruggero.caravita@cern.ch (R. Caravita), mariazzi@science.unitn.it (S. Mariazzi).

https://doi.org/10.1016/j.nimb.2019.07.015
Received 12 April 2019; Received in revised form 20 June 2019; Accepted 15 July 2019
Available online 30 July 2019
0168-583X/

tronium excited to a selected state and characterizing its spatial distribution is discussed. Ways to further improve the spatial resolution of the method are presented.

1. Introduction

Positronium (Ps), the bound state of an electron and its antiparticle (positron, e^+), is a purely leptonic matter/antimatter atom that constitutes a privileged system for high-precision studies of Quantum Electrodynamics (QED) and for matter/antimatter symmetry studies [1]. Ps has a central role in the study of matter-antimatter gravitational interactions. On one hand, Ps has been identified as a promising intermediate system for antihydrogen production via a charge-exchange reaction with an antiproton [2–4]. Specifically, the AEgIS [5–7] and GBAR collaborations [8] are exploring the possibility of producing antihydrogen following the charge-exchange reaction scheme to experimentally probe the antimatter gravitational acceleration. Moreover, Ps, previously excited to long-lived states like Rydberg levels [9,10] or 2^3S level [11], has been proposed as candidate for direct measurements of free-fall.

For all the mentioned applications, it would be of great help to have a high spatial-resolution position sensitive detector for slow Ps. Indeed, it would allow monitoring the Ps emission from e^+/Ps converters [12–17], it would be a quick diagnostic tool for Ps laser excitation experiments, it would permit the fast characterization in terms of transport and focus of a long-lived Ps beam [18–20] and, in the future, it could be employed in force-sensitive inertial experiments with Ps as test particle to detect and measure the fringe pattern generated by a deflectometer/interferometer device [11].

A widely used method for localizing positron annihilation events, which could be employed to determine the Ps impact position on a surface, is Positron Emission Tomography (PET) [21,22]. PET detectors are typically based on the coincidence detection of the anti-parallel photons emitted by e^+ annihilation. The Ps impact position can be determined by acquiring the coincidence annihilation photons generated by Ps pick-off annihilation (annihilation of the e^+ of Ps with an electron of the medium), extracting the line of response (LOR) along which the annihilation took place and finally determining the interception of the LOR with the impact plane. The spatial resolution of similar devices is mainly determined by the physical size of the employed detector elements and is typically larger than 0.5 mm (Full Width Half Maximum) [23,24]. However, this technique is designed to handle single Ps atoms and it cannot be applied in experiments employing large numbers of Ps atoms in few ns pulses like in the case of antihydrogen production [5,8] and several experiments of Ps spectroscopy [1].

To directly detect the impact position of Ps, a Microchannel Plate (MCP) can be used in case the Ps kinetic energy is higher than several eV [25,26]. This excludes the possibility of directly imaging slow Ps and imposes to ionize the incident atoms and then collect the freed e^+ or e^- onto the MCP [27]. Up to now, MCPs coupled to an ionizing system have been used to count the approaching Ps atoms excited to Rydberg states with the aim to perform high energy-resolution Time Of Flight measurements [27].

In the present work, we describe a position sensitive detector for bunches of slow Ps. The detector is based on a MCP – phosphor screen assembly, housed in a magnetic field, and a 2-photon resonant ionization laser with ns-long pulses. After ionization of Ps with laser pulses, the freed e^+ and e^- (photo-e^+ and photo-e^-) are bound to their magnetic field line, thus conserving the original Ps position in the plane transverse to the magnetic field at the ionization instant. Positrons are then guided towards the front face of the MCP –perpendicular to the field– while electrons are repelled by negatively biasing the surface. The spatial distribution of e^+ impinging the MCP front face –and consequently the spatial distribution of the ionized Ps in the plane transverse to the field– is imaged. The detector has been tested on a Ps cloud produced in the 1.0 T field of the AEgIS experiment [5–7].

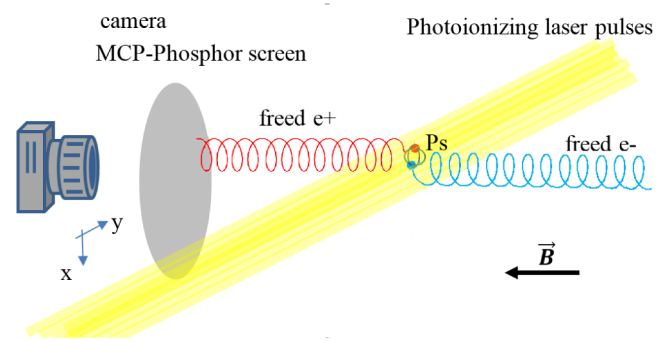

Fig. 1. Schematic of the position sensitive Ps detection scheme. Ps is photoionized via laser pulses. The photo-e^+ drifts along the magnetic field lines towards the negatively biased surface of the MCP. This drift conserves the original position of the Ps in the x-y plane (see text).

2. Detector

2.1. General principle

The detection principle of the present detector is schematically represented in Fig. 1.

A given Ps atom can be photoionized through a 2-photon resonant process. Specifically, Ps can be excited to n = 2 [28] or n = 3 [29] level with a first laser pulse and then selectively photoionized with a second laser pulse. If photoionization occurs in a homogeneous magnetic field, the freed e^+ and e^- remain bound by the Lorentz force to the magnetic field lines, following a cyclotron movement with the diameter d [Eq. (1)]:

$$d = \frac{2mv}{qB}, \tag{1}$$

where m and q are the e^+/e^- mass and charge (in absolute value), respectively and v the component of the velocity perpendicular to the magnetic field $\vec{B}$. This means that, in the plane perpendicular to the magnetic field, the charged particles move away from the original Ps position by less than the distance d. If an MCP assembly is then placed with its front face perpendicular to the magnetic field, the impact position of the photo-e^+ or photo-e^- can be imaged and thus the position of the photoionized Ps in the plane transverse to the field (x-y in Fig. 1) can be determined.

By applying a bias voltage to the metallized surface of the MCP one has the possibility to select positive or negative species [30]. For the present application, detecting positrons only is definitely preferable. Indeed they can uniquely come from the Ps photoionization while electrons can be extracted from the surface of the experimental chamber also by the employed laser pulses via photoemission. Thus the use of e^+ guarantees a better backgroud suppression. The bias voltage of the MCP front face has also the advantage of increasing the longitudinal component of the particles' velocity and thus the detection efficiency of the MCP [31].

2.2. Used detector

The detection system used in the present test, performed in the AEgIS apparatus, is made of:

(i) a Hamamatsu F2222 two-stage MCP assembly with a P46 phosphor screen imaged by a Hamamatsu ORCA-Flash4 CMOS camera. The MCP surface has been biased to −180 V to repel electrons and to attract only freed e^+. MCP out was set at 1.2 kV and the phosphor screen at 4.2 kV. An optical lens system composed of three plano-convex uncoated fused-silica lenses (Lens 1: diameter D = 51 mm, distance from the phosphor screen z = 305 mm, focal length f = 85 mm; Lens 2: D = 75 mm, z = 320 mm, f = 250 mm; Lens 3: D = 75 mm, z = 580 mm, f = 250 mm) is installed in the vacuum on the back of the MCP assembly to provide efficient light collection. This lens system is coupled to a commercial 105 mm f2.8 optics on the camera, mounted on an adjustable rail, to provide optimal magnification of the phosphor screen surface.

(ii) A 1.0 T magnetic field with homogeneity better than [32–34] surrounding the MCP assembly and the source of Ps with the vector $\vec{B}$ perpendicular to the front face of the MCP assembly.

(iii) an UV pulse (wavelength tunable between 204.9 and 205.2 nm, nearly Gaussian temporal profile with a full-width at half maximum (FWHM) of 1.5 ns, and a Gaussian-like spectral profile with $\sigma_{UV} = 2\pi \times 120 GHz$, energy of 50 μJ) to induce the Ps $1^3S \rightarrow 3^3P$ transition plus a simultaneous IR pulse (1064 nm, temporal FWHM of 6 ns, energy of 60 mJ) to selectively photoionize Ps on the 3^3P level. A more detailed description of the laser system can be found in [29,35].

Positron bursts are produced using the AEgIS positron system described in Ref.[36]. The bursts are then implanted in a e^+/Ps converter made of Si with oxidized nanochannels [14,37] placed in the 1.0 T field. The converter is tilted with an angle of 30° with respect to the magnetic field direction and is placed 15 cm upstream of the front face of the MCP. Thus, the Ps atoms, emerging from the nanochannels, are not in the view of the MCP in the very first part of their free flight as they are hidden by the target (see Fig. 2). The atoms that overcome the target edge come in view of the MCP and the e^+ freed by the laser pulses can drift unobstructed along the magnetic field lines to the MCP where they are imaged.

The Ps detection efficiency of the present scheme is given by three terms:

- the UV + IR ionization efficiency that amounts up to ∼ 15%[29], being mainly limited by the UV laser bandwidth, because with the intense IR pulse almost all atoms excited to the 3^3P level are found to be photoionized [29].
- the transport efficiency of the photo-e^+ to the MCP. In the present configuration, photo-e^+ are emitted in a solid angle of 4π sr and only the fraction in the half-space of the MCP is guided by the magnetic field towards its surface. The transport efficiency is consequently ∼ 50%.
- the detection efficiency of the MCP that for photo-e^+ with an impinging energy of 180 eV is expected to be ∼ 50%[31,38].

The overall detector efficiency results to be ∼ 4% of the produced Ps atoms.

The spatial resolution of the present detector is expected to be determined by three main parameters: (a) the cyclotron orbit diameter in the magnetic field in the region between the MCP and the point where Ps is photoionized, (b) the intrinsic resolution of the MCP-assembly and (c) the resolution of the imaging system. The orbit diameter of the photo-e^+/ photo-e^-(point a) is determined by the component of their velocity transversal to the magnetic field [Eq. (1)]. This velocity can be estimated by considering that the first UV laser pulse populates the 3^3P level which has a binding energy of the order of $-6.8\ eV/(n=3)^2 = -0.76$ eV. The following 1064 nm IR laser pulse adds 1.16 eV. Therefore, the freed e^+ and e^- divide the final energy of $(-0.76 + 1.16)eV = 0.4$ eV. The initial kinetic energy of the Ps atom is expected to give a small contribution of the order of a few tens of meV [29]. The velocity of each dissociated charged particle is thus expected to be of the order of few 10^5 m/s. By applying Eq. (1), one finds that the diameter of the orbits of e^+ and e^- around the magnetic field lines, in the described detection system, is <3 μm.

The intrinsic resolution of the MCP assembly (point b) is set by the interdistance of the MCP micro-channels and by the distance and the potential difference between the phosphor screen and the MCP which determine the spot size on the phosphor screen of the electrons emerging from the MCP. In the case of our two-stage assembly, it is expected to be of the order of 80–100 μm [31].

The magnification of the MCP, lens system and camera assembly (point c) has been experimentally measured by imaging a reference of 10.00 mm placed in the converter region. A maximum magnification of 43.6 pixel/mm, corresponding to a spatial sampling resolution of ∼ 23 μm per pixel, has been found.

3. Imaging of Ps photoionization position

In order to determine the resolution of the detector, we aligned the center of the UV spot (FWHM = 3.4 mm) with the bottom edge of the target. Thus, the UV pulse addresses both Ps atoms in view of the MCP and Ps hidden by the target (see Fig. 2). The UV pulse has been shot t = (15 ± 3) ns after the e^+ implantation to the converter with a wavelength λ = 205.045 nm (± $\Delta\lambda$ = 16.8 pm, due to the spectral profile described above). The laser pulse selects Ps atoms with a module of the velocity along the laser direction (v_{Ps-y}) determined by the following equation [Eq. (2)]:

$$v_{Ps-y} = c\left(\frac{\lambda_0}{\lambda} - 1\right), \tag{2}$$

where λ_0 is the UV wavelength corresponding to the resonance of the $1^3S \rightarrow 3^3P$ transition (205.045 nm) [29]. The y-position of Ps can be roughly estimated as $y = v_{Ps-y}t$. The simultaneous IR laser pulse is superimposed to the UV spot with a larger diameter of FWHM = 6 mm. The used energy of the IR pulse ensures the saturation of the photoionization from the 3^3P level [29]. The spatial distribution –in the plane transverse to the 1.0 T magnetic field– of photo-e^+, as imaged by the MCP assembly, is reported in Fig. 3.

The dark region in the upper part of the picture (negative-x) is due to the shadow of the target while the bright part below (positive-x) is given by photo-e^+ able to reach the MCP-assembly. The bright signal reproduces, along the y-axis, the distribution of the Ps velocity component v_{Ps-y}. The sharp edge of the target is expected to generate a step transition between the two regions that, in this measurement, is smoothed by the spatial resolution of the detector. The spatial resolution of our detector can thus be estimated by analyzing the transition from the absence of signal to the maximum intensity of the image of

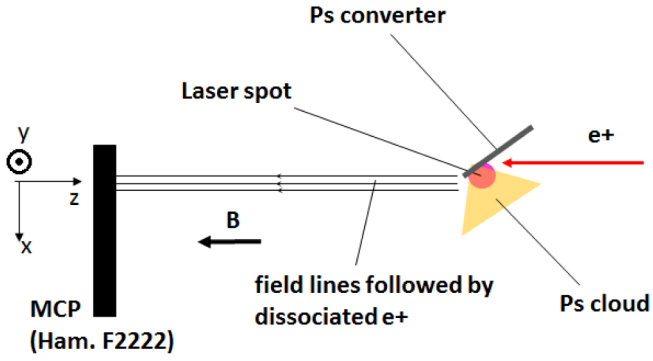

Fig. 2. Schematic side view of the used detection system in the 1.0 T magnetic field of AEgIS. The position of the Ps converter, the Ps cloud, laser spot and MCP are indicated. The lasers are shot along the y-axis. The black arrows depict the path of the dissociated e^+ from the Ps photoionization.

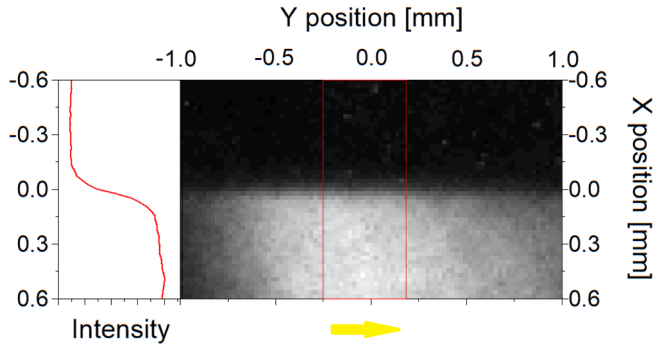

Fig. 3. Image of spatial distribution in the plane transverse to the 1.0 T field (x-y plane) of e^+ freed by Ps photoionization. The border between the dark and the bright regions in the picture corresponds to the lower edge of the e+/Ps converter. The yellow arrow indicates the lasers direction. The intensity profile along the x-axis –calculated in the indicated red perimeter– is shown on the left of the image (see text for the details). (For interpretation of the references to colour in this figure legend, the reader is referred to the web version of this article.)

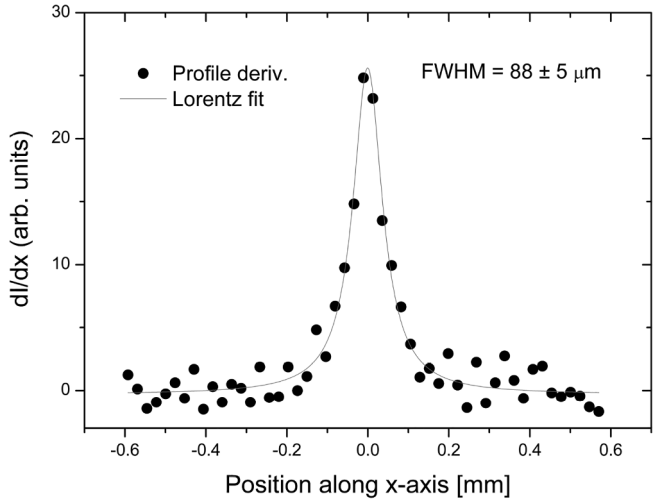

Fig. 4. Derivative of the intensity profile of the image shown in Fig. 3 as a function of x-position in the region indicated in Fig. 3. The continuous line is the best Lorentzian fit of the data.

Fig. 3. The intensity of the image has been integrated in y in the marked region. The obtained plot of the intensity I as a function of the x-position is reported in the left panel of Fig. 3.

The derivative of the intensity profile and its best Lorentzian fit are shown in Fig. 4. The transition from the no-signal to the maximum intensity region has been found to occur in (88 ± 5) μm FWHM. This value is in very good agreement with the expected spatial resolution of the MCP-assembly of 80–100 μm [31] confirming that this is the main factor in the determination of the overall resolution of the detector.

We notice that, one could apply the present scheme also in lower and more accessible magnetic fields than the 1.0 T used here. Indeed, according to Eq. (1), a field of 0.05 T ensures orbits of the photo-e^+ still smaller than 25 μm. Thus, a total spatial resolution of $\sqrt{25^2 + 88^2}$ μm ~ 90 μm can be achieved opening the possibility to apply the present detection scheme in other contexts than the complex and dedicated AEgIS system.

As an application of this Ps imaging system, we have changed the UV laser wavelengths in the range between 204.99 to 205.10 nm keeping the other experimental conditions as above. The so excited 3^3P state was then photoionized by the IR pulse. As pointed out by Eq. (2), changing the UV wavelength allows to perfom Doppler selection of Ps with different v_{Ps-y} ranges. The measurements are shown in Fig. 5. The spatial distribution of the bright spots reflects this velocity selection. By setting the UV pulse on the 1^3S-3^3P transition resonance ($\lambda = \lambda_0$), Ps with roughly null v_{Ps-y}, and thus traveling along the x-axis, can be selected. The detune of the wavelength induces the selection of Ps with larger v_{Ps-y} component that is imaged in the position $y = v_{Ps-y}t$.

In the context of the AEgIS experiment, a scan of this type –thanks to the relatively high efficiency of the MCP assembly for e^+ with few hundreds of eV of energy [31,38]– takes few minutes and it allows monitoring the main parameters necessary for the production of a Ps beam and for experiments of Ps laser excitation. In particular, it permits to monitor the Ps emission from the e^+/Ps converter, the Ps/laser synchronization and the Ps excitation to a selected state. Moreover, the possibility to make visible the direction of propagation of the fraction of Ps excited to the 3^3P state allows performing a fine tuning of the central wavelength of the UV pulse to select the velocity component aiming in a specific direction.

4. Conclusion

In this work, we have presented the concept of a slow Ps high-resolution position-sensitive detection scheme based on a MCP – phosphor screen assembly, housed in a magnetic field, and ns-long 2-photon resonant ionization laser pulse. Such a detector has been tested in the 1.0 T magnetic field of the AEgIS experiment. An overall detection efficiency of ~ 4% with respect to the produced Ps atoms is obtained. This value is close to the ~ 6% efficiency demonstrated for field ionization of Ps previously excited to Rydberg levels (where a 10% of $1^3S\rightarrow$ Rydberg

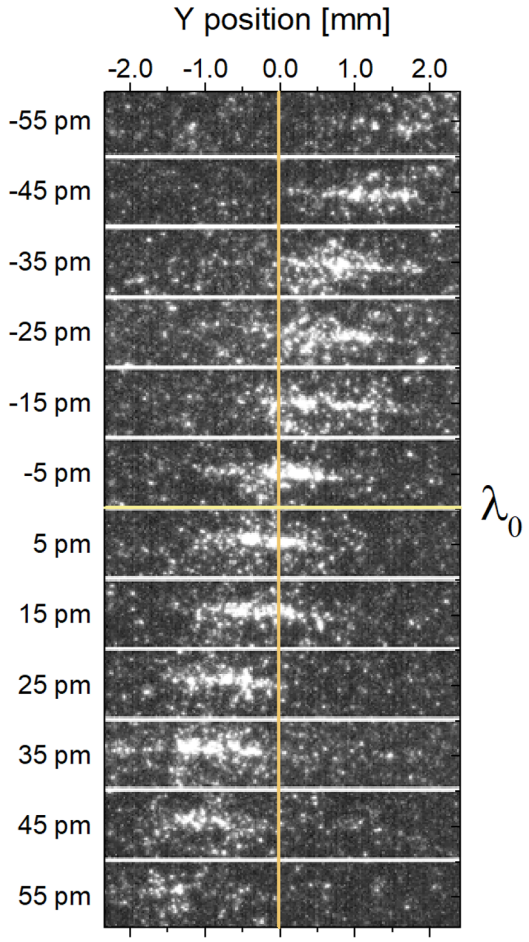

Fig. 5. images of spatial distribution in the plane transverse to the 1.0 T field (x-y plane, see Fig. 2) of e^+ freed by Ps photoionization. Each image corresponds to different wavelengths of the UV laser pulse. The detune of the wavelength with respect to λ_0 is reported on the left side.

excitation efficiency has been assumed and a ∼ 60% of overall field ionization, freed-e^+ transport and detection efficiency with an MCP has been estimated) [27].

The efficiency of the present detector could be improved by the introduction of a potential of few tens of eV placed upstream the ionization region to reflect the photo-e^+ not emitted in the half-space of the MCP. With this expedient, the transport efficiency of photo-e^+ towards the MCP could approach 100%. Moreover, the detection efficiency of the MCP could be enhanced up to ∼ 85% by biasing the MCP surface to $-2kV$ [31,38]. With these improvements, an overall efficiency of ∼ 13%(=15% × 100% × 85%) could be reached.

A spatial resolution of (88 ± 5) μm for the e^+ impinging the MCP front face, and consequently on the position of the ionized Ps in the plane perpendicular to the 1.0 T magnetic field, has been demonstrated. The present detector allows performing a spatially precise and quick monitoring of Ps emission into vacuum from e^+/Ps converters, Ps laser excitation and Ps transport. This novel tool can thus be helpful in all the experiments where there is the need to create and transport a Ps beam [7,9–11]. We plan to apply the described detector to characterize emission angle and velocity distribution of Ps emitted by different kinds of e^+/Ps converters. An improvement of the performances of the presented detection scheme could be obtained by employing a single-stage MCP-assembly that is expected to reduce the spatial resolution to 40–50 μm [31]. A further reduction of the spatial resolution at values lower than 10 μm could be obtained, in the case of low density Ps clouds, by employing MCPs with small pores and methods for the centroid reconstruction [39].

Acknowledgments

This work was supported by Istituto Nazionale di Fisica Nucleare; the CERN Fellowship programme and the CERN Doctoral student programme; the Swiss National Science Foundation Ambizione Grant (No. 154833); a Deutsche Forschungsgemeinschaft research grant; an excellence initiative of Heidelberg University; Marie Sklodowska-Curie Innovative Training Network Fellowship of the European Commission's Horizon 2020 Programme (No. 721559 AVA); European Research Council under the European Unions Seventh Framework Program FP7/2007-2013 (Grant Nos. 291242 and 277762); European Union's Horizon 2020 research and innovation programme under the Marie Sklodowska-Curie grant agreement ANGRAM No. 748826; Austrian Ministry for Science, Research, and Economy; Research Council of Norway; Bergen Research Foundation; John Templeton Foundation; Ministry of Education and Science of the Russian Federation and Russian Academy of Sciences and the European Social Fund within the framework of realizing Research infrastructure for experiments at CERN, LM2015058.

References

[1] D.B. Cassidy, Experimental progress in positronium laser physics, Eur. Phys. J. D 72 (2018) 53.
[2] M. Charlton, F.M. Jacobsen, B.I. Deutch, J. Phys. B 20 (1987) L25.
[3] M. Charlton, Antihydrogen production in collisions of antiprotons with excited states of positronium, Phys. Lett. A 143 (3) (1990) 143.
[4] C.H. Storry, A. Speck, D.L. Sage, N. Guise, G. Gabrielse, D. Grzonka, W. Oelert, G. Schepers, T. Sefzick, H. Pittner, M. Herrmann, J. Walz, T.W. Hänsch, D. Comeau, E.A. Hessels, First laser-controlled antihydrogen production, Phys. Rev. Lett. 93 (2004) 263401.
[5] A. Kellerbauer, et al., Proposed antimatter gravity measurement with an antihydrogen beam, Nucl. Instrum. Methods Phys. Res., Sect. B 266 (2008) 351–356.
[6] R.S. Brusa, et al., (AEgIS collaboration), The AEgIS experiment at CERN: measuring antihydrogen free-fall in earth's gravitational field to test WEP with antimatter, J. Phys.: Conf. Ser. 791 (2017) 012014.
[7] M. Doser, et al., Exploring the WEP with a pulsed cold beam of antihydrogen, Classical Quantum Gravity 29 (18) (2012) 183009.
[8] P. Perez, et al., GBAR collaboration, Hyperfine Interact. 233 (2015) 21.
[9] A.P.j. Mills, M. Leventhal, Can we measure the gravitational free fall of cold Rydberg state positronium? Nucl. Instr. Meth. Phys. Res. B 192 (2002) 102–106.
[10] D.B. Cassidy, S.D. Hogan, Atom control and gravity measurements using Rydberg positronium, Int. J. Modern Phys.: Conf. Ser. 30 (2014) 1450259.
[11] M.K. Oberthaler, Anti-matter wave interferometry with positronium, Nucl. Instr. Meth. Phys. Res. B 192 (2002) 129.
[12] A.P. Mills, E.D. Shaw, M. Leventhal, R.J. Chichester, D.M. Zuckerman, Thermal desorption of cold positronium from oxygen-treated al(111) surfaces, Phys. Rev. B 44 (1991) 5791–5799.
[13] L. Liszkay, C. Corbel, P. Perez, P. Desgardin, M. Barthe, T. Ohdaira, R. Suzuki, P. Crivelli, U. Gendotti, A. Rubbia, M. Etienne, A. Walcarius, Positronium reemission yield from mesostructured silica films, Appl. Phys. Lett. 92 (2008) 063114.
[14] S. Mariazzi, P. Bettotti, S. Larcheri, L. Toniutti, R.S. Brusa, High positronium yield and emission into the vacuum from oxidized tunable nanochannels in silicon, Phys. Rev. B 81 (23) (2010) 235418.
[15] D.B. Cassidy, T.H. Hisakado, H.W.K. Tom, A.P. Mills, Photoemission of positronium from si, Phys. Rev. Lett. 107 (2011) 033401.
[16] A.C.L. Jones, H.J. Goldman, Q. Zhai, P. Feng, H.W.K. Tom, A.P. Mills, Monoenergetic positronium emission from metal-organic framework crystals, Phys. Rev. Lett. 114 (2015) 153201.
[17] S. Aghion, et al., (AEgIS collaboration), Characterization of a transmission positron/positronium converter for antihydrogen production, Nucl. Instrum. Methods Phys. Res., Sect. B 407 (2017) 55–66.
[18] A.C.L. Jones, J. Moxom, H.K. Rutbeck-Goldman, K.A. Osorno, G.G. Cecchini, M. Fuentes-Garcia, R.G. Greaves, D.J. Adams, H.W.K. Tom, A.P. Mills, M. Leventhal, Phys. Rev. Lett. 119 (2017) 053201.
[19] A.M. Alonso, B.S. Cooper, A. Deller, L. Gurung, S.D. Hogan, D.B. Cassidy, Velocity selection of rydberg positronium using a curved electrostatic guide, Phys. Rev. A 95 (2017) 053409.
[20] C. Amsler, et al., (AEgIS collaboration), Velocity-selected production of 2^3s metastable positronium, Phys. Rev. A 99 (2019) 033405.
[21] T.K. Lewellen, Recent developments in pet detector technology, Phys. Med. Biol. 53 (2008) 287.
[22] P. Kowalski, W. Wiślicki, R.Y. Shopa, L. Raczyński, K. Klimaszewski, C. Curcenau, E. Czerwiński, K. Dulski, A. Gajos, M. Gorgol, N. Gupta-Sharma, B. Hiesmayr, B. Jasińska, D. Kapłon, G. Kisielewska-Kamińska, T. Korcyl, W. Kozik, E. Krzemień, M. Kubicz, S. Mohammed, M. Niedźwiecki, M. Pałka, J. Pawlik-Niedźwiecka, K. Raj, K. Rakoczy, S. Rudy, S. Sharma, M. Shivani, M. Silarski, B. Skurzok, M. Zgardzińska, P. Moskal Zieliński, Estimating the nema characteristics of the j-pet tomograph using the gate package, Phys. Med. Biol. 63 (2018) 165008.
[23] W.W. Moses, Fundamental limits of spatial resolution in pet, Nucl. Inst. Method A 648 (2011) S236–S240.
[24] Y. Yang, J. Bec, J. Zhou, M. Zhang, M.S. Judenhofer, X. Bai, K.D. Yibao Wu, M. Rodriguez, P. Dokhale, K.S. Shah, R. Farrell, J. Qi, S.R. Cherry, A prototype high-resolution small-animal pet scanner dedicated to mouse brain imaging, J. Nucl. Med. 57 (7) (2016) 1130–1135.
[25] A.P. Mills, W.S. Crane, Beam-foil production of fast positronium, Phys. Rev. A 31 (1985) 593–597.
[26] D.W. Gidley, R. Mayer, W.E. Frieze, K.G. Lynn, Glancing angle scattering and neutralization of a positron beam at metal surfaces, Phys. Rev. Lett. 58 (1987) 595–598.
[27] A.C.L. Jones, A.M. Piñeiro, E.E. Roeder, H.J. Rutbeck-Goldman, H.W.K. Tom, A.P. Mills, Large-area field-ionization detector for the study of rydberg atoms, Rev. Sci. Instrum. 87 (11) (2016) 113307.
[28] D.B. Cassidy, T.H. Hisakado, H.W.K. Tom, A.P. Mills, Efficient production of Rydberg positronium, Phys. Rev. Lett. 108 (2012) 043401.
[29] S. Aghion, et al., (AEgIS collaboration), Laser excitation of the n = 3 level of positronium for antihydrogen production, Phys. Rev. A 94 (2016) 012507.
[30] A. Camper, et al., (AEgIS collaboration), Imaging a positronium cloud in a 1 tesla, EPJ Web Conf. 198 (2019) 00004.
[31] Hamamtsu, Mcp assembly: technical information, https://www.triumf.ca/sites/default/files/Hamamatsu%20MCP%20guide.pdf.
[32] A. Dudarev, M. Doser, D. Perini, H. ten Kate, Design of a superconducting magnet system for the aegis experiment at cern, IEEE Trans. App. Supercond. 21 (2011) 1721.
[33] A. Dudarev, J. Bremer, G. Burghart, L. Deront, M. Doser, H. ten Kate, D. Perini, F. Restuccia, S. Ravat, T. Winkler, Construction and test of the magnets for the aegis experiment, IEEE Trans. App. Supercond. 22 (2012) 4500304.
[34] J.H. Derking, J. Bremer, G. Burghart, M. Doser, A. Dudarev, S. Haider, Development of the cryogenic system of aegis at cern, AIP Conf. Proceed. 1573 (2014) 195.
[35] S. Aghion, et al., (AEgIS collaboration), Producing long-lived 2^3s ps via 3^3p laser excitation in magnetic and electric fields, Phys. Rev. A 98 (2018) 013402.
[36] S. Aghion, et al., (AEgIS collaboration), Positron bunching and electrostatic transport system for the production and emission of dense positronium clouds into vacuum, Nucl. Instrum. Methods Phys. Res., Sect. B 362 (2015) 86–92.
[37] S. Mariazzi, P. Bettotti, R.S. Brusa, Positronium cooling and emission in vacuum from nanochannels at cryogenic temperature, Phys. Rev. Lett. 104 (24) (2010) 243401.
[38] G.B. Andresen, W. Bertsche, P.D. Bowe, C.C. Bray, E. Butler, C.L. Cesar, S. Chapman, M. Charlton, S.S. El Nasr, J. Fajans, M.C. Fujiwara, D.R. Gill, J.S. Hangst, W.N. Hardy, R.S. Hayano, M.E. Hayden, A.J. Humphries, R. Hydomako, L.V. Jorgensen, S.J. Kerrigan, L. Kurchaninov, R. Lambo, N. Madsen, P. Nolan, K. Olchanski, A. Olin, A.P. Povilus, P. Pusa, E. Sarid, D.M. Silveira, J.W. Storey, R.I. Thompson, D.P. van der Werf, Y. Yamazaki, A. Collaboration, Antiproton, positron, and electron imaging with a microchannel plate/phosphor detector, Rev. Sci. Inst. 80 (12) (2009) 123701.
[39] A.S. Tremsin, J.V. Vallerga, J.B. McPhate, O.H.W. Siegmund, Optimization of high count rate event counting detector with microchannel plates and quad timepix readout, Nucl. Instrum. Methods Phys. Res., Sect. A 787 (2015) 20.